First-principles study of polar LaAlO (001) surface stabilization by point defects

Hosung Seo and Alexander A. Demkov

Phys. Rev. B **84**, 045440 — Published 22 July 2011

DOI: 10.1103/PhysRevB.84.045440

First-principles study of polar $LaAlO_3$ (001) surface stabilization by point defects

Hosung Seo and Alexander A. Demkov*
Department of Physics, The University of Texas at Austin, Austin, Texas 78712, USA

Abstract

We use density functional theory to investigate the influence of surface vacancies on the surface stability of a stoichiometric free-standing $LaAlO_3$ (001) thin film. Defect-free three and five unit cell thick $LaAlO_3$ (001) thin films show macroscopic electric fields of 0.28 V/Å and 0.22 V/Å, respectively. The built-in electric field is sufficiently strong for the five unit cell thick film to undergo a dielectric breakdown in the local density approximation. We show that the electric field can be effectively compensated by La vacancies on the LaO surface, O vacancies on the AlO_2 surface, or both types of vacancy present at the same time. Comparing surface Gibbs free energies we show that several surface vacancy structures are thermodynamically stable.

1. Introduction

Lanthanum aluminate $LaAlO_3$ (LAO) is a polar perovskite oxide widely used as a single crystal substrate material in oxide epitaxy [1,2]. Along the [001] direction LAO can be viewed as a stack of alternating charged LaO and AlO_2 planes. In the ionic limit, the LaO and AlO_2 planes carry a charge of +e and –e per (1×1) in-plane cell, respectively. Therefore, an ideal as-cleaved LAO film would have an electrostatic potential diverging as the film thickness increases. In the semiconductor context the effect is known as polar catastrophe [3]. Recently, thin films of LAO have drawn considerable attention owing to the discovery of the two-dimensional electron gas in the $LaAlO_3/SrTiO_3$ (STO) heterostructure [4-14]. Several studies of oxide heterostructures including LAO layers have followed [15-18]. In many cases, the intrinsic polarity of LAO is believed to be responsible for novel physical phenomena. The built-in electric field may offer, for example, a possible explanation for the interfacial charge and critical thickness of the LAO overlayer in the LAO/STO system. Electrons transfer from the valence band at the LAO surface to the conduction band of the STO substrate as the film thickness exceeds 4 unit cells [7,8]. This model explains the main properties of the LAO/STO system; however, it assumes that the LAO surface maintains its defect-free structure.

The key question is whether the as-cleaved LAO (001) surface can be kept to sustain the built-in electric field. Harrison has shown that the polar catastrophe can be avoided when the surface

* demkov@physics.utexas.edu

atomic composition is modified so that accumulated charge is compensated [3]. The idea can be readily applied to the polar oxide surface. When bulk LAO is stoichiometrically cleaved, positively charged LaO and negatively charged AlO_2 surfaces are exposed. If one can introduce compensating charges, for example, -δ to the LaO surface and +δ to the AlO_2 one, this gives in the simple capacitor model compensating electric field of $4\pi\delta/\varepsilon$ inside the LAO film, where ε is the dielectric constant of LAO. This surface charge compensation can be achieved, for instance, by desorbing native ions or adsorbing foreign charged entities on the surface [19]. The LAO (001) surface has been extensively studied both theoretically and experimentally [20-32]. Several point defects in bulk LAO and O vacancies in LAO (001) film have been studied theoretically [33-36]. Using density functional theory Zhang *et al*.[35] have recently shown that O vacancy preferably forms at the AlO_2 surface of the LAO overlayer on STO. Zhong *et al.*, have discussed the similar position dependence of formation energy of an O vacancy in the LAO/STO superlattice [36]. La vacancies on the LaO-terminated surface of LAO (001) film have been observed experimentally using a transmission electron diffraction technique [30]. Using density functional theory Lanier *et al*. have theoretically evaluated the basic electronic properties of the LaO surface with a La vacancy [30]. However, to our knowledge, the details of the stabilization mechanism for the LAO (001) polar surface have not been considered theoretically. In this paper we use first-principles calculations to study the stability of the built-in electric field in LAO (001) films with respect to formation of surface vacancies. The rest of the paper is organized as follows. We briefly describe the computational methods in section 2. In section 3, we discuss defect-free three unit-cell (u.c.) and five u.c. thick LAO (001) films. We consider five u.c. thick LAO (001) thin films with three different surface vacancy structures in section 4. Surface Gibbs free energy and relative thermodynamic stability of the vacancy structures are discussed in section 5.

2. Computational methods

We use density functional theory (DFT) within the local density approximation (LDA) as implemented in the VASP code [37]. The exchange-correlation functional is approximated using parameterization by Perdew and Zunger [38]. We employ projector augmented wave (PAW) pseudopotentials [39] to describe La, Al, and O. Valence configurations for the elements are $5s^2 5p^6 5d^1 6s^2$ for La, $3s^2 3p^1$ for Al, and $2s^2 2p^4$ for O. A plane wave cutoff energy of 600 eV is used, along with a 8×8×8 (bulk) and a 6×6×2 (slab) Monkhorst-Pack special k-point grids [40] for integration over the Brillouin zone. The electronic total energy is converged within 10^{-6} eV/cell for each electronic self-consistent field calculation. Experimentally, the

ground state structure of LAO below 820K is a rhombohedral perovskite ($R\bar{3}c$) with the tilted AlO_6 octahedra network [41-44]. We calculate the rhombohedral cell angle α in the ground state structure to be 60.1°. We note that this value is very close to 60° corresponding to cubic symmetry of the system (see FIG. 1 (a)), and energy difference between the α=60° and α=60.1° structures is less than 0.5 meV/(LAO-formula-unit). Therefore in what follows we approximate the ground state structure of LAO with the cubic perovskite structure with tilted octahedra. In FIG. 1 (b), we plot the energy of bulk LAO as a function of the rotation angle φ of the octahedra about the cubic [111] direction. The ground state angle is found to be 6.1° in good agreement with the experimental value of 5.7° at 4.2K [44]. We compare several ground state properties of bulk LAO calculated in this work to previous theoretical results and available experimental data in TABLE 1.

We consider free-standing, stoichiometric LAO (001) slabs having two chemically different (LaO and AlO_2) surfaces as shown in FIG. 2. The cell size is 2×2. Since the slab is stoichiometrically terminated, there is a potential difference across the film due to the built-in electric field. To deal with the electric field within the periodic boundary condition, we use double-slab geometry to produce a periodic potential [7]. Three u.c. and five u.c. thick LAO (001) films are considered. We define a layer of LaO plus a layer of AlO_2 as one u.c.. Therefore thicknesses of the as-cleaved three u.c. and five u.c. films are 9.37 Å and 16.86 Å, respectively. The LAO slabs in the simulation cell are separated by 10 Å thick vacuum regions. To ensure that the vacuum thickness is large enough to avoid spurious interactions between the slabs, we check that the electrostatic potential is flat in the vacuum region for each result. We have also considered one three u.c. thick LAO (001) slab structure using 15 Å of vacuum, and checked that it gives the same result as one obtained with 10 Å of vacuum. We fully relax all slab structures until the Hellmann-Feynman forces are less than 25 meV/Å.

3. Defect-free $LaAlO_3$ (001) films

We first examine the as-cleaved stoichiometric three u.c. thick film. To study the electronic and ionic responses of the system to the built-in electric field separately, we first consider the un-relaxed structure. We show the layer-projected density of states (DOS) of the cleaved-bulk structure in FIG. 3 (a). The main feature is tilt of the LAO band structure due to the built-in electric field. The valence band states of the AlO_2 layer on the right are raised in energy so that they reach the conduction band level of the LaO layer on the left. The electrons in the valence states of the AlO_2 layer can tunnel through the film and transfer into the LaO layer, rendering the film metallic. This is a dielectric breakdown. We calculate the electric field using planar average of the local electrostatic potential by plotting it as a function of distance in the direction

normal to the surface in FIG. 3 (b). The potential is then macroscopically averaged along the stacking direction and the electric field is estimated from the slope in the bulk region. The field in the un-relaxed three u. c. thick film is 0.39 V/Å. Next we allow the atoms to relax. As seen in FIG. 4 (a) and (c), La and Al cations move to the right and O anions move to the left with respect to their bulk positions. Note that the residual electric field is pointing toward the AlO_2 surface, so the ions move to screen it. This 'polar-type' distortion in the three u.c. thick LAO film reduces the electric field to 0.28 V/Å. As a result the system opens the band gap of 1.18eV and returns to an insulating state. Similar polar distortions in LAO/STO heterostructures have also been discussed by Pentcheva and Pickett [8].

To further analyze the system's response, we calculate layer charges based on the Bader analysis [45,46]. The Bader method partitions the continuous charge density into atomic charges based on the so-called zero flux surfaces on which the charge density is minimal in the direction normal to the surface. Since LAO is largely ionic, the Bader method is a natural choice to assign the atomic charges. We use the number of electrons per (2x2) in-plane cell as a unit for the charge density unless noted otherwise. In the bulk, the Bader charges of the LaO and AlO_2 bulk layers are calculated to be 1.43e and -1.43e, respectively (in the ionic limit they would have been 4e and -4e). As shown in FIG. 5 (a), the middle LaO and AlO_2 layers in the three u.c. thick film are charged approximately 1.45e, and -1.45e, respectively, before and after the structural relaxation. Major changes take place in the surface regions. For the cleaved-bulk structure, the surface charges are 0.9e and -0.9e for the LaO and AlO_2 surfaces, respectively. Note, however, that in the original model of Hwang [4] the charge transfer would have been 2e in the cell of this size, and the field would be gone. In other words, what we observe is the inability of the electron system alone to alleviate the polar catastrophe. Once the ions are allowed to relax and the ionic dipoles are induced, the electric field is further screened and the charge transfer leading to the dielectric breakdown vanishes. The Bader charge of the surface layer is now roughly +/-2e (See FIG. 5 (a)). The higher surface charges can be understood within a simple bond electron transfer model [19]. In this model the ionic formal charges are corrected by the electron transfer due to orbital hybridization with the nearest neighbors. For example, the atomic charges of La, Al, and O in the bulk are given by $Q_{La} = 3 - 12\Delta_{La\text{-}O}$, $Q_{Al} = 3 - 6\Delta_{Al\text{-}O}$, and $Q_O = -2 + 4\Delta_{La\text{-}O} + 2\Delta_{Al\text{-}O}$, where $\Delta_{La\text{-}O}$ and $\Delta_{Al\text{-}O}$ are amounts of electron transfer from O to La and Al, respectively. Using the Bader charges of La, Al, and O in the bulk we estimate that $\Delta_{La\text{-}O} \approx 0.08$ and $\Delta_{Al\text{-}O} \approx 0$. The transition nature of La manifests in a larger correction than that of Al, despite the larger electronegativity difference (EN(O)=3.44, EN(Al)=1.61 and EN(La)=1.1). Considering the coordination environment at the surfaces and Δ values in the bulk, the surface charges are estimated to be +2.6e and -2.6e for LaO and AlO_2 surfaces, respectively, in qualitative agreement with the calculated values. We conclude that the residual electric field of 0.28 V/Å is a result of balancing between the charge transfer and ionic screening. Most importantly, we find that at least in very thin films, the dielectric breakdown can be averted.

For a five unit cell thick film, the dielectric breakdown is also observed for the cleaved-bulk geometry as seen in FIG. 6 (a). The relaxed structure shows a polar distortion similar to that of the relaxed three unit cell thick film (see FIG. 4 (b) and (c)). However, unlike the thinner film, the thicker one cannot avoid the dielectric breakdown even after the polar distortion, and both surfaces remain metallic. This can be also observed in the layer-resolved Bader charge plot shown in FIG. 5 (b). Again, the surface charge accumulation is enhanced by the ionic relaxation. However, the values (1.81e and -1.46e for the LaO and AlO_2 surfaces, respectively) are smaller than for the three unit cell thick film, meaning that the initial electronic charge transfer doesn't vanish. This charge transfer additionally reduces the electric field by 0.06 V/Å in comparison to the three unit cell case, and the residual electric field is 0.22 V/Å.

In summary, we find that above the critical thickness of about four unit cells, an ideal stoichiometric LAO film cannot avoid the dielectric breakdown as electrons transfer from the O 2p states at the AlO_2-surface to the La 5d states at the opposite LaO-surface. We see from the three unit cell thick film result that the electric field in the bulk region of LAO is 0.28 V/Å. Therefore, because the LDA band gap of LAO is only 3.87 eV the critical thickness is only ~14 Å. However, the LDA is known to under-estimate the band gap [49]. The experimental band gap of LAO is 5.6eV. Using the electric field of 0.28 V/Å, the critical thickness is estimated to be 20 Å or five unit cells.

4. Thin $LaAlO_3$ (001) films with surface vacancies

To explore the residual electric field stability with respect to point defects we consider three different surface vacancy structures: 1) (1/4)-monolayer (ML) of La vacancies on the LaO surface, 2) (1/8)-ML of O vacancies on the AlO_2 surface, and 3) (1/4)-ML of La vacancies on the LaO together with (1/8)-ML of O vacancies on the AlO_2 surface (mixed vacancies). An Al vacancy at the AlO_2 surface and O vacancy at the LaO surface are not considered because they are not expected to compensate the surface charge. For example, a neutral O vacancy at the LaO surface would produce two electrons localized at the surface leaving the overall charge unchanged. A similar argument applies in the case of a neutral Al vacancy at the AlO_2 surface. The initial slab geometry is taken from the fully relaxed, defect-free five u.c. thick LAO slab and vacancies are created by removing atoms from the surfaces as shown in FIG. 7. The vacancies are neutral so that the LAO films remain neutral after the vacancy formation. We have considered several vacancy concentrations, the results are qualitatively similar to the lower concentration cases discussed in this section.

We compare the macroscopically averaged electrostatic potential in the presence of vacancies before and after the structural relaxation. The results for each vacancy structure are shown in

FIG. 8. First, we observe that the built-in electric field in the bulk region is readily influenced by the surface vacancy formation even before the ionic relaxation. In particular, for the un-relaxed LAO film with the La surface vacancies, the residual electric field is only 0.03 V/Å. Other vacancies also significantly reduce the electric field, leaving the residual fields of 0.11 V/Å and -0.12 V/Å for the O vacancy case and the mixed vacancy one, respectively. When we allow for the ionic relaxation, the electric field is further screened and reduced to zero in the bulk region for all cases. We plot the layer-projected density of states for each structure in FIG. 9. Due to the compensation of the electric field in the presence of the surface vacancies, no band tilting can be observed. Energy gaps of 3.65eV, 2.85eV, and 3.31eV open up for the La, O, and mixed vacancy case, respectively. There are, however, important differences between the La and O vacancies. The La surface vacancies induce hole states at the top of the valence band (O 2p states) as shown in FIG. 9 (a). Creating O vacancies involves breaking the Al-O bonds and releases electrons. The surface states pinning the Fermi level inside the band gap are clearly seen in the projected density of states (see FIG. 9 (b)). The exact energy position of the defect level is difficult to ascertain at the LDA level since the state is localized and self-interaction may push it higher up in energy [50]. Xiong *et al*. have studied the neutral O vacancy in LAO bulk using the screened exchange method and found that the neutral O vacancy induces a singly degenerate gap state lying 0.8 eV below the conduction band, trapping two electrons [33].

The defect-related charges play a crucial role in screening of the built-in electric field. We compare layer-resolved Bader charges of the LAO films having the surface vacancies to that of the fully relaxed defect-free five u.c. LAO film in FIG. 10. If no relaxation is allowed, there is only the electronic response of the system. The main effect occurs within the first two layers away from the surface at which the vacancies are created. For the La vacancies (see FIG. 10. (a)) the holes reduce the charges of the LaO surface and the adjacent AlO_2 layer from 1.81e to 0.89e and from -1.41e to -0.74e, respectively. The electrons introduced by the O surface vacancies at the AlO_2 surface modify the Bader charges of the AlO_2 surface from -1.46e to -1.05e and that of the adjacent LaO layer from 1.06e to 0.75e as shown in FIG. 10 (b). When the mixed vacancies are created, holes are introduced at the LaO surface and electrons at the opposite AlO_2 surface. Similar to the La and O vacancy cases, the holes and electrons are 'localized and polarized' mainly in the surface regions where they are created as shown in FIG. 10 (c). This happens because there are no available states in the bulk region or at the opposite LaO surface to accept the electrons generated by an O surface vacancy at the AlO_2 surface (for the holes introduced by the La surface vacancies that would be the AlO_2 surface).

Once the ions are allowed to relax, for example in the case of the LAO film with the La surface vacancies, additional surface states appear at the top of the valence band at the opposite AlO_2 surface (see FIG. 9 (a)). These states accommodate the holes transferred from the LaO surface. This screening process is also seen in the Bader charges in FIG. 10 (a). The Bader charges of the LaO and AlO_2 surfaces are further compensated to 0.25e and -0.73e, respectively, due to the hole transfer after the ionic relaxation. Ionic relaxation in the LAO film with the O surface vacancies creates additional surface states at the bottom of the conduction band of the LaO surface as seen in FIG. 9 (b). The electrons localized at the AlO_2 surface before the relaxation transfer to these new states. This leads to further reduction of the Bader charges of the LaO and AlO_2 surfaces to 0.93e and -0.62e, respectively as shown in FIG. 10 (b). For the mixed vacancy case, the electrons at the AlO_2 surface and the holes at the LaO surface are transferred to the opposite sides. The surface charges are reduced to 0.20e for the LaO and to -0.45e for the AlO_2 surface after ionic relaxation.

It is interesting to note that in the presence of surface vacancies the polar distortion disappears and the bulk region recovers the tilted perovskite structure. Relative atomic displacements for each case are presented in FIG. 11. In the bulk region La atoms are close to their centrosymmetric positions, the O atoms of the LaO planes move close to the bulk positions, and O atoms of the AlO_2 planes show rumpling characteristic of the octahedral tilting in bulk LAO [9]. The polar-distortion is energetically costly because all Al-O bonds are distorted. Once the system has available screening charges, the role of the ionic dipoles diminishes. Instead, the system induces surface states by having a local surface distortion and screens the built-in electric fields by filling these states. Pauli *et al.* have recently reported the structural evolution of LAO on STO as the LAO film thickness increases from two to five unit cells using surface x-ray diffraction techniques [11]. They find that the buckling of the LaO planes indicative of the polar distortion disappears when the film thickness exceeds four unit cells. Our result suggests that this disappearing of buckling is an indication of the polar surface stabilization by screening. The actual screening mechanism may of course be different from the one described here due to the presence of the epitaxial interface with STO. We hope that further experimental studies of the atomic-scale evolution of the LAO surface structure will shed light on this complicated problem. Lastly we notice that the surface structure we obtain for the AlO_2 surface is in qualitative agreement with the experimental result of Francis *et al.* [27]. They reported the outward relaxation of O atoms and inward relaxation of Al atoms for the AlO_2-terminated LAO (001) surface.

5. Stability of surfaces with vacancies

Thus far we have established that by having surface vacancies, the LAO film could reduce the built-in electric field and lower its energy by recovering the bulk tilted perovskite lattice. The surface vacancy formation, however, costs a certain amount of energy. If the energy cost to create surface vacancies is too high, then the energy gain due to the compensation of the built-in electric field may not be sufficient to have an appropriate vacancy concentration. To compare the stability of the surfaces with vacancies to that of the stoichiometric LAO (001) surface we calculate the surface Gibbs free energy for each structure, defined as

$$\Omega = \frac{1}{2}[E(slab) - N_{La}(\mu_{La} + E_{La}^{bulk}) - N_{Al}(\mu_{Al} + E_{Al}^{bulk}) - N_O(\mu_O + \frac{1}{2}E_{O_2}^{molecule})], \quad (1)$$

where E(slab) is the total energy of the LAO slab under consideration. N_{La}, N_{Al}, and N_O, are the numbers of La, Al, and O atoms in the slab, respectively. The chemical potentials for the elements μ_{La}, μ_{Al}, and μ_O are referenced to bulk metals, and O_2 molecule. We approximate the Gibbs free energy of the slabs as the total energy obtained from the DFT calculations; that is, the vibrational and pressure contributions to free energy are neglected [51].

Since the surface is assumed to be in equilibrium with the LAO bulk, the sum of the chemical potentials should satisfy the equilibrium condition:

$$\mu_{La} + \mu_{Al} + 3\mu_O = \Delta E_f^{LAO}, \quad (2)$$

where $\Delta E_f^{LAO} \equiv E_{LAO}^{bulk} - E_{La}^{bulk} - E_{Al}^{bulk} - \frac{3}{2}E_{O_2}^{molecule}$ is the formation energy of LAO bulk.

Using this relation, we can reduce the number of independent variables in the surface free energy expression from three to two.

$$\Omega = \frac{1}{2}[E(slab) - N_{Al}E_{LAO}^{bulk}] - \Gamma_{La,Al}E_{La}^{bulk} - \Gamma_{O,Al}(\frac{1}{2}E_{O_2}^{molecule}) - \Gamma_{La,Al}\mu_{La} - \Gamma_{O,Al}\mu_O, \quad (3)$$

where $\Gamma_{La,Al} = \frac{1}{2}(N_{La} - N_{Al})$ and $\Gamma_{O,Al} = \frac{1}{2}(N_O - 3N_{Al})$.

There are additional boundary conditions for the chemical potentials:

$$\mu_{La} \le 0 \text{ and } \mu_{Al} \le 0, \quad (4)$$

$$2\mu_{La} + 3\mu_O \le \Delta E_f^{La_2O_3} \text{ and } 2\mu_{Al} + 3\mu_O \le \Delta E_f^{Al_2O_3}, \quad (5)$$

where $\Delta E_f^{La_2O_3(Al_2O_3)} = E_{La_2O_3(Al_2O_3)}^{bulk} - 2E_{La(Al)}^{bulk} - \frac{3}{2}E_{O_2}^{molecule}$ are the formation energies of binary oxides. These conditions guarantee that any bulk metal precipitation and formation of the binary oxides are prohibited.

Combining conditions (2), (4), and (5), we obtain the following ranges of possible values of chemical potentials:

$$2\Delta E_f^{LAO} - \Delta E_f^{Al_2O_3} \le 2\mu_{La} + 3\mu_O \le \Delta E_f^{La_2O_3} \qquad (6)$$

$$\Delta E_f^{LAO} \le \mu_{La} + 3\mu_O \qquad (7)$$

We list the calculated formation energies for bulk $LaAlO_3$, La_2O_3, and Al_2O_3 in Table 2. Theoretical values are in good agreement with experiment.

Based on these formation energies, we determine the relevant chemical potential ranges and build the surface phase diagram as shown in FIG. 12. As can be seen in the figure, the binary oxide La_2O_3 would precipitate on the LAO surface for the chemical potential values above the La_2O_3 precipitation line, and Al_2O_3 would precipitate below the Al_2O_3 precipitation line. There is an Al precipitation line below which the bulk Al metal would form at the surface. All surface energies are compared inside the strip defined by three precipitation lines. Zero values of chemical potential correspond to La-rich and O-rich limits. The phase diagram shown in FIG. 12 is drawn as follows. We include the surface if its free energy is lower than that of the stoichiometric LAO film. If there are multiple stable surface vacancy structures, we indicate the surface with the lowest surface free energy in the diagram. For example, in the strip region, the surface with 1/8-ML of O vacancies becomes stable when the O chemical potential is less than -4.6 eV. As approaching the O-poor condition for the O chemical potential (lower than -5.8 eV) the 1/4-ML of O vacancies becomes more stable than the 1/8-ML of O vacancy structure. The surface with mixed vacancies and the one with La vacancies are stable when the La chemical potential is reduced beyond -6.3 eV in the strip. The most interesting result is that in the range of intermediate values of La and O chemical potentials the LAO (001) film of thickness larger than critical (five u.c. thick film in LDA) could have stable stoichiometric surfaces and maintain the built-in electric field of 0.22 V/Å. We finally remark that the phase diagram constructed in FIG. 12 considers a limited portion of the phase space. There may be, depending on different chemical and physical environment, other types of defects present such as

molecular adsorbates or extended defects stabilizing the LAO thin film. These would require further theoretical and experimental investigations.

6. Summary

In conclusion, we use first-principles density functional theory calculations to explore the possible mechanism of LAO (001) polar surface stabilization. All considered defect-free stoichiometric LAO (001) thin films suffer the dielectric breakdown in the as-cleaved geometry. The three u.c. thick film could screen the electric field by a strong polar-type distortion, leading to the insulating phase with the built-in electric field of 0.28 V/Å. However, already a five u.c. thick LAO (001) film cannot avoid the charge transfer from the valence band states of AlO_2 surface to the conduction band states of the LaO surface. The built-in electric field in the bulk region of the relaxed five u.c. thick LAO (001) film is calculated to be 0.22 V/Å. We find that surface vacancies readily compensate the built-in electric field. The creation of La and O surface vacancies induces holes and electrons, respectively. Vacancies cause large structural relaxation that creates gap states at the surface to accommodate these charges. This screens the electric field. These local surface distortions are less costly energetically than the global polar-type distortion maintaining the compensating ionic dipoles. The defective film recovers the tilted perovskite structure in the bulk region. Comparing the surface Gibbs free energy of different surfaces, we show that several surface vacancy structures are thermodynamically stable in the certain range of the La and O chemical potentials. We also find that, there is a narrow chemical potential range in which the polar stoichiometric (001) surface is stable and therefore can sustain the built-in electric field.

This work is supported by the National Science Foundation under grant DMR-0548182, the US Department of Energy (DOE) under grant DE-SC0001878, and Texas Advanced Computing Center.

References

[1] R. W. Simon, C. E. Platt, A. E. Lee, G. S. Lee, K. P. Daly, M. S. Wire, J. A. Luine, and M. Urbanik, Appl. Phys. Lett. **53**, 2677 (1988).

[2] A. Masuno, M. Haruta, M. Azuma, H. Kurata, S. Isoda, M. Takano, and Y. Shimakawa, Appl. Phys. Lett. **89**, 211913 (2006).

[3] W. A. Harrison, E. A. Kraut, J. R. Waldrop, and R. W. Grant, Phys. Rev. B **18**, 4402 (1978).

[4] A. Ohtomo and H. Y. Hwang, Nature (London) **427**, 423 (2004).

[5] S. Thiel, G. Hammerl, A. Schmehl, C. W. Schneider, J. Mannhart, Science **313**, 1942 (2006).

[6] N. Nakagawa, H. Y. Hwang, and D. A. Muller , Nat. Mater. **5**, 204 (2006).

[7] J. K. Lee and A. A. Demkov, Phys. Rev. B. **78**, 193104 (2008).

[8] R. Pentcheva and W. E. Pickett, Phys. Rev. Lett. **102**, 107602 (2009).

[9] C. L. Jia, S. B. Mi, M. Faley, U. Poppe, J. Schubert, and K. Urban, Phys. Rev. B **79**, 081405(R) (2009).

[10] Y. Segal, J. H. Ngai, J. W. Reiner, F. J. Walker, and C. H. Ahn, Phys. Rev. B **80**, 241107(R) (2009).

[11] S. A. Pauli, S. J. Leake, B. Delley, M. Björck, C. W. Schneider, C. M. Schlepütz, D. Martoccia, S. Paetel, J. Mannhart, and P. R. Willmott, Phys. Rev. Lett. **106**, 036101 (2011)

[12] J. Mannhart and D. G. Schlom, Science **327**, 1607 (2010)

[13] H. Chen, A. M. Kolpak, and S. Ismail-Beigi, Advanced Materials **22**, 2881 (2010)

[14] M. Huijben, A. Brinkman, G. Koster, G. Rijnders, H. Hilgenkamp, and D. H. A. Blank, Advanced Materials **21**, 1665 (2009)

[15] M. Takizawa, Y. Hotta, T. Susaki, Y. Ishida, H. Wadati, Y. Takata, K. Horiba, M. Matsunami, S. Shin, M. Yabashi, K. Tamasaku, Y. Nishino, T. Ishikawa, A. Fujimori, and H. Y. Hwang, Phys. Rev. Lett. **102**, 236401 (2009)

[16] S. S. A. Seo, M. J. Han, G. W. J. Hassink, W. S. Choi, S. J. Moon, J. S. Kim, T. Susaki, Y. S. Lee, J. Yu, C. Bernhard, H. Y. Hwang, G. Rijnders, D. H. A. Blank, B. Keimer, and T. W. Noh, Phys. Rev. Lett. **104**, 036401 (2010)

[17] Y. Wang, M. K. Niranjan, J. D. Burton, J. M. An, K. D. Belashchenko, and E. Y. Tsymbal, Phys. Rev. B **79**, 212408 (2009)

[18] J. K. Lee, N. Sai and A. A. Demkov, Phys. Rev. B **82**, 235305 (2010).

[19] J. Goniakowski, F. Finocchi, and C. Noguera, Rep. Prog. Phys. **71**, 016501 (2008).

[20] Z. L. Wang and A. J. Shapiro, Surf. Sci. **328**, 141 (1994).

[21] Z. L. Wang and A. J. Shapiro, Surf. Sci. **328**, 159 (1994).

[22] Z. L. Wang, Surf. Sci. **360**, 180 (1996).

[23] J. Yao, P. B. Merrill, S. S. Perry, D. Marton, and J. W. Rabalais, J. Chem. Phys. **108**, 1645 (1997).
[24] J. Jacobs, M. A. S. Miguel, and L. J. Alvarez, J. of Molec. Struc. **390**, 193 (1997).
[25] J. Jacobs, M. A. S. Miguel, J. E. Sánchez-Sánchez, and L. J. Alvarez,, Surf. Sci. **389**, L1147 (1997).
[26] P. A. W. van der Heide and J. W. Rabalais, Chem. Phys. Lett. **297**, 350 (1998).
[27] R. J. Francis, S. C. Moss, and A. J. Jacobson, Phys. Rev. B **64**, 235425 (2001).
[28] H. Kawanowa, H. Ozawa, M. Ohtsuki, Y. Gotoh, and R. Souda, Surf. Sci. **506**, 87 (2002).
[29] A. Asthagiri and D. S. Sholl, Phys. Rev. B **73**, 125432 (2006).
[30] C. H. Lanier, J. M. Rondinelli, B. Deng, R. Kilaas, K. R. Poeppelmeier, and L. D. Marks, Phys. Rev. Lett. **98**, 086102 (2007).
[31] J. Tang, J. Zhu, W. Qin, J. Xiong, Y. Zhang, and Y. Li, Phys. Lett. A **365**, 149 (2007).
[32] A. A. Knizhnik, I. M. Iskandarova, A. A. Bagatur´yants, B. V. Potapkin, L. R. C. Fonseca, and A. Korkin, Phys. Rev. B **72**, 235329 (2005).
[33] K. Xiong, J. Robertson, and S. J. Clark, Appl. Phys. Lett. **89**, 022907 (2006).
[34] X. Luo, B. Wang, Y. Zheng, Phys. Rev. B **80**, 104115 (2009).
[35] L. Zhang, X. Zhou, H. Wang, J. Xu, J. Li, E. Wang, and S. Wei, Phys. Rev. B **82**, 125412 (2010)
[36] Z. Zhong, P. X. Xu, and P. J. Kelly, Phys. Rev. B **82**, 165127 (2010)
[37] G. Kresse and J. Furthmüller, Phys. Rev. B **54**, 11169 (1996).
[38] J. P. Perdew and A. Zunger, Phys. Rev. B **23**, 5048 (1981).
[39] P. E. Blöchl, Phys. Rev. B **50**, 17953 (1994).
[40] H. J. Monkhorst and J. D. Pack. Phys. Rev. B **13**, 5188 (1976).
[41] S. Geller and V. B. Bala, Acta Crystallogr. **9**, 1019 (1956)
[42] K. A. Müller, W. Berlinger, and F. Waldner, Phys. Rev. Lett. **21**, 814 (1968)
[43] A. M. Glazer, Acta Cryst. B **28**, 3384 (1972).
[44] S. A. Hayward, F. D. Morrison, S. A. T. Redfern, E. K. H. Salje, J. F. Scott, K. S. Knight, S. Tarantino, A. M. Glazer, V. Shuvaeva, P. Daniel, M. Zhang, and M. A. Carpenter, Phys. Rev. B **72**, 054110 (2005).
[45] R. F. W. Bader, *Atoms in Molecules: A Quantum Theory* (Clarendon, Oxford, 1990).
[46] W. Tang, E. Sanville, and G. Henkelman, J. Phys.: Condens. Matter **21**, 084204 (2009).
[47] M. A. Carpenter, S. V. Sinogeikin, J. D. Bass, D. L. Lakshtanov, and S. D. Jacobsen, J. Phys.: Condens. Matter **22**, 035403 (2010).
[48] P. Delugas, V. Fiorentini, and A. Filippetti, Phys. Rev. B **71**, 134302 (2005).
[49] L. J. Sham and M. Schlüter, Phys. Rev. Lett. **51**, 1888 (1983).

[50] S. Lany and A. Zunger, Phys. Rev. B **78**, 235104 (2008).

[51] K. Reuter and M. Scheffler, Phys. Rev. B **65**, 035406 (2001).

[52] W. Schnelle, R. Fischer, and E. Gmelin. J. Phys. D **34**, 846 (2001).

[53] S. Lim, S. Kriventsov, T. N. Jackson, J. H. Haeni, D. G. Schlom, A. M. Baldashov, R. Uecker, P. Reiche, J. L. Freeouf, G. Lucovsky, J. Appl. Phys. **91**, 4500 (2002).

[54] CRC Handbook of Chemistry and Physics, 90th ed., CRC Press: Boca Raton, FL. 2009-2010.

Tables

TABLE 1. Bulk properties of $LaAlO_3$

	a (Å)	E_g (eV)	α (°)	φ (°)
Theory (This work)	5.29	3.87	60.1	6.1
Theory (DFT-LDA)	5.31[a]	3.3[a]	60.2[b]	6.3[b]
Experiments	5.36 (4.2K)[c]	5.6[d]	60.15 (4.2K)[c]	5.7 (at 4.2K)[c]

[a]Reference 32.

[b]Reference 48.

[c]Reference 44.

[d]Reference 53.

TABLE 2. Formation energies per formula unit.

Material	Theory, LDA (eV)	Expt. (eV)
$LaAlO_3$	-18.94	-17.25[a]
La_2O_3	-19.03	-18.58[b]
Al_2O_3	-17.49	-17.36[b]

[a]Reference 52.

[b]Reference 54.

Figure captions

FIG. 1. (Color online) (a) Rhombohedral unit cell of $LaAlO_3$. The unit cell vectors are designated as $\vec{a}_1$, $\vec{a}_2$ and $\vec{a}_3$. α = 60° is used and the corresponding cubic perovskite cells are shown with black boxes. The [001] and [111] indicate the crystallographic directions of the cubic cell. (b) Total energy versus octahedral tilting angle in $LaAlO_3$. The lowest total energy is set to 0 eV.

FIG. 2. (Color online) The simulation cell: two five u.c. thick LAO (001) slabs in the cell are mirror-symmetric.

FIG. 3. (Color online) (a) Layer-projected density of states of the three u.c. thick LAO film. The Fermi level is located at 0 eV. Planar-averaged local electrostatic potential energy of the three u.c. LAO film before relaxation (b) and after relaxation (c), respectively. The vacuum level between the AlO_2 surfaces is set to 0 eV. The macroscopically averaged potential energies are shown by blue curves.

FIG. 4. (Color online) Side views of the relaxed structure of the three u.c. LAO film (a), and the relaxed structure of the five u.c. LAO film (b). (c) Relative displacements of the ions with respect to the La and Al (001) planes in the bulk LAO.

FIG. 5. (Color online) Bader charges of LaO and AlO_2 layers in the three u.c. thick LAO film (a), and in the 5 u.c. thick LAO film (b).

FIG. 6. (Color online) (a) Layer-projected density of states of the five u.c. thick LAO film. The Fermi level is located at 0 eV. Planar-averaged local electrostatic potential energy of the five u.c. thick LAO film before relaxation (b) and after relaxation (c), respectively. The vacuum level between the AlO_2 surfaces is set to 0 eV. The macroscopically averaged potential energies are shown by blue curves.

FIG. 7. (Color online) Schematic of the surface vacancies.

FIG. 8. (Color online) Planar-averaged electrostatic potential of the five u.c. thick LAO films with (1/4)-ML of La vacancies (a), (1/8)-ML of O vacancies (b), and mixed vacancies (c).

FIG. 9. Layer-projected density of states of the five u.c. thick LAO film with (1/4)-ML of La vacancies (a), (1/8)-ML of O vacancies (b), and mixed vacancies (c). The Fermi energy is located at 0 eV. Gray dotted lines show the projected density of states before relaxation and black lines show the projected density of states after relaxation.

FIG. 10. (Color online) Bader charges of LaO and AlO_2 layers in the five u.c. thick LAO film with (1/4)-ML of La vacancies (a), (1/8)-ML of O vacancies (b), and mixed vacancies (c).

FIG. 11. (Color online) Relative displacements of atoms in the five u.c. thick LAO (001) slab with (1/4)-ML of La vacancies (a), (1/8)-ML of O vacancies (b), and mixed vacancies (c) with respect to the La and Al (001) planes in the bulk LAO structure.

FIG. 12. (Color online) Phase diagram for the LAO (001) surface as a function of La and O chemical potentials.

Figures

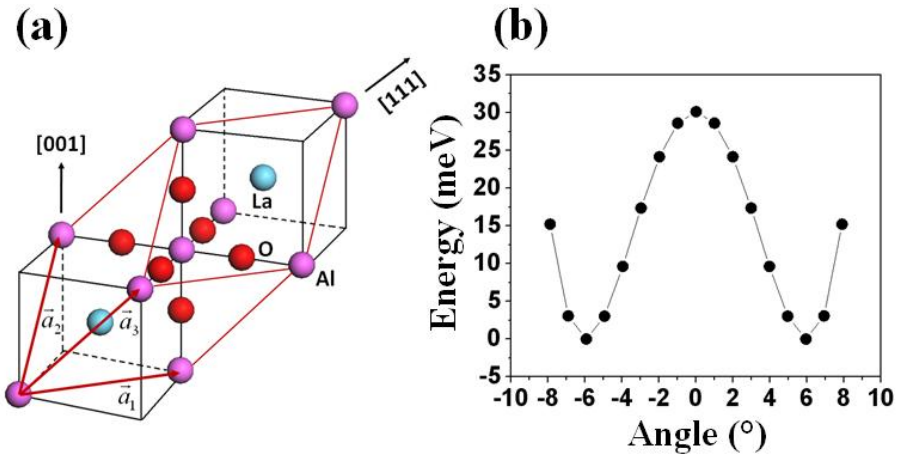

FIG. 1.

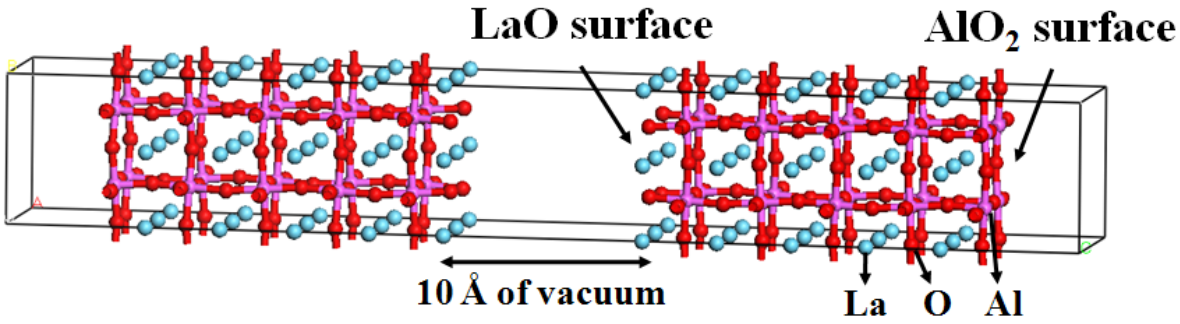

FIG. 2.

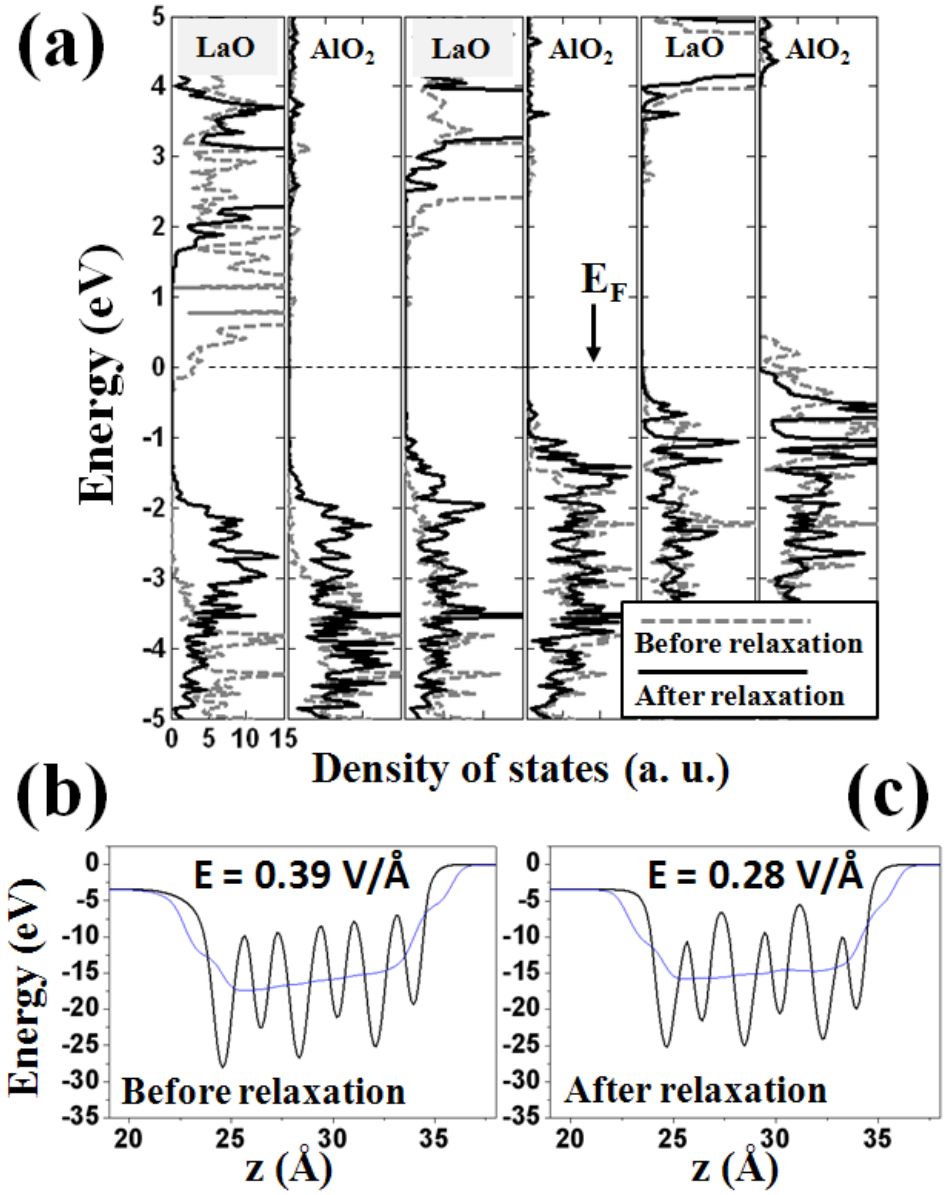
(a)
LaO
AlO2
LaO
AlO2
LaO
AlO2
EF
Energy (eV)
Density of states (a. u.)
Before relaxation
After relaxation
(b)
(c)
E = 0.39 V/Å
E = 0.28 V/Å
Before relaxation
After relaxation
Energy (eV)
z (Å)
z (Å)

FIG. 3.

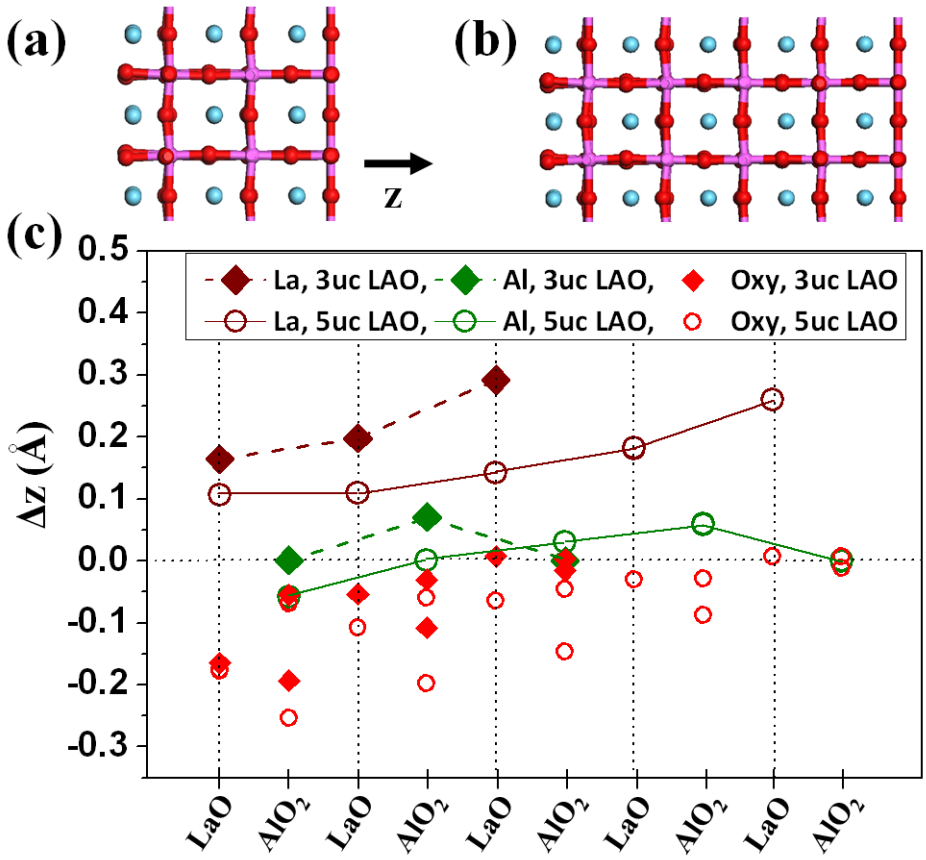
(a)
(b)
z
(c)
La, 3uc LAO,
Al, 3uc LAO,
Oxy, 3uc LAO
La, 5uc LAO,
Al, 5uc LAO,
Oxy, 5uc LAO
Δz (Å)
0.5
0.4
0.3
0.2
0.1
0.0
-0.1
-0.2
-0.3
LaO
AlO2

FIG. 4.

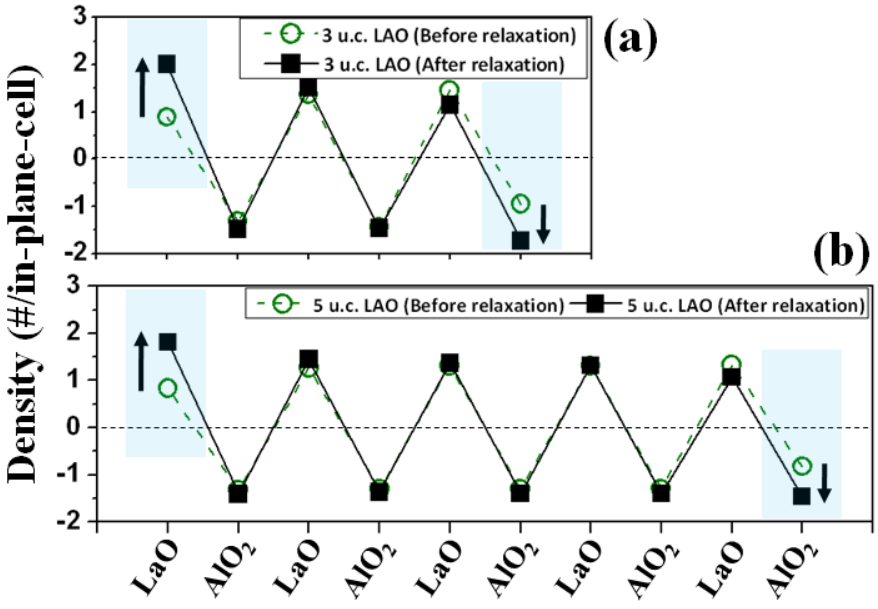
3 u.c. LAO (Before relaxation)
3 u.c. LAO (After relaxation)
(a)
(b)
5 u.c. LAO (Before relaxation)
5 u.c. LAO (After relaxation)
Density (#/in-plane-cell)
3
2
1
0
-1
-2
LaO
AlO2

FIG. 5.

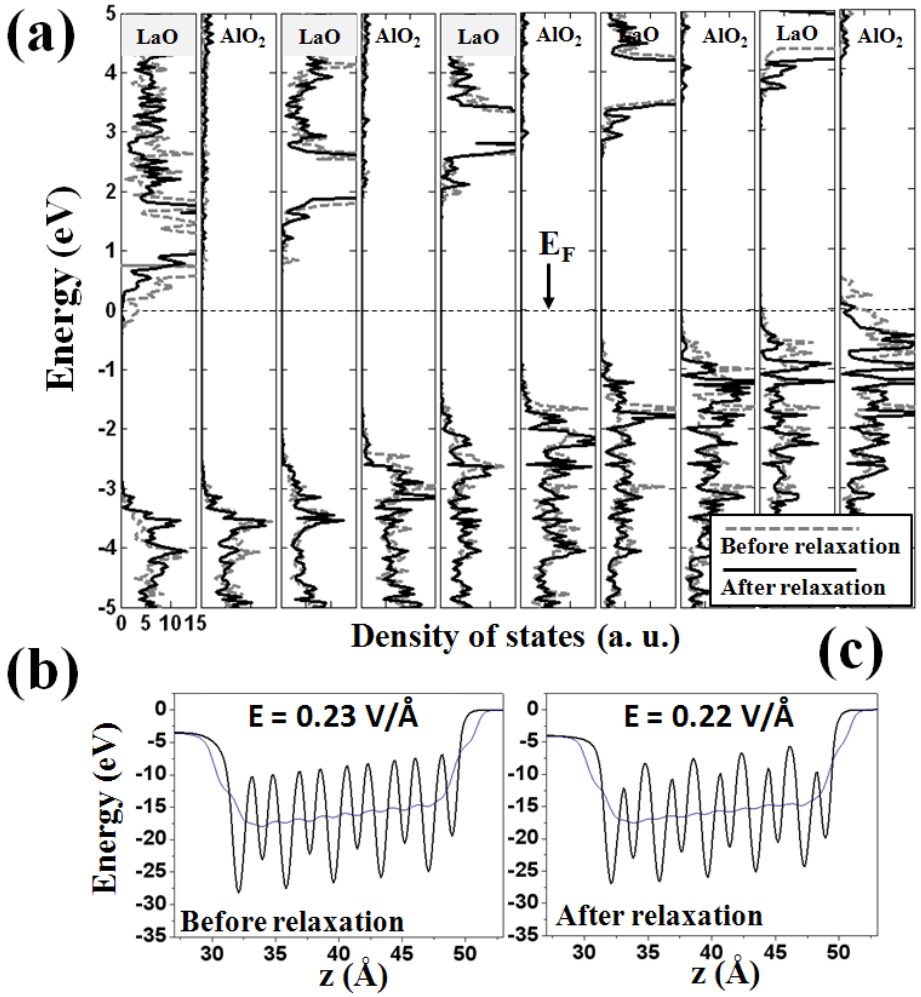
(a)
LaO
AlO2
LaO
AlO2
LaO
AlO2
LaO
AlO2
LaO
AlO2
Energy (eV)
E_F
Before relaxation
After relaxation
Density of states (a. u.)
(b)
(c)
E = 0.23 V/Å
E = 0.22 V/Å
Energy (eV)
Before relaxation
After relaxation
z (Å)
z (Å)

FIG. 6.

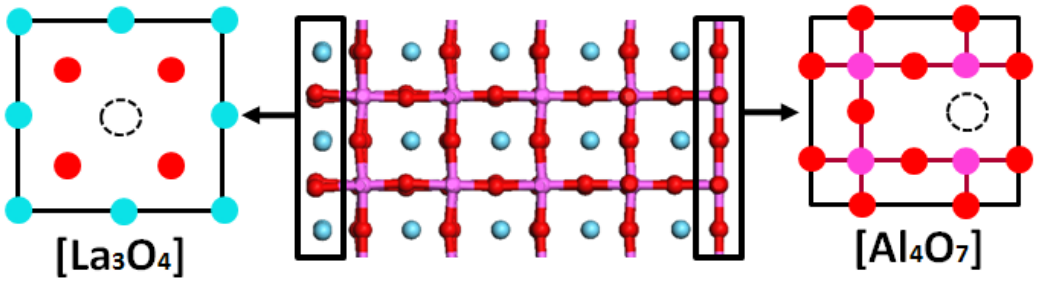
[La3O4]
[Al4O7]

FIG. 7.

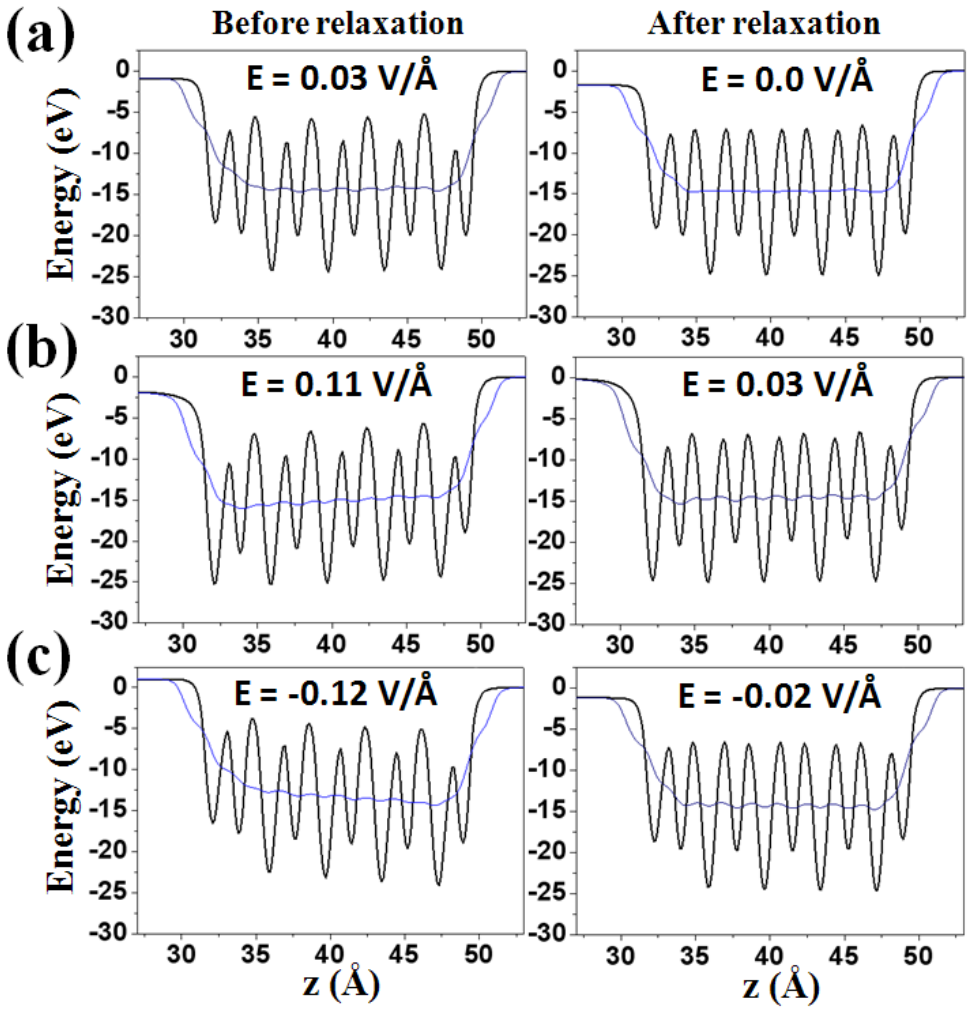
(a)
Before relaxation
After relaxation
E = 0.03 V/Å
E = 0.0 V/Å
(b)
E = 0.11 V/Å
E = 0.03 V/Å
(c)
E = -0.12 V/Å
E = -0.02 V/Å
Energy (eV)
0
-5
-10
-15
-20
-25
-30
30
35
40
45
50
z (Å)

FIG. 8.

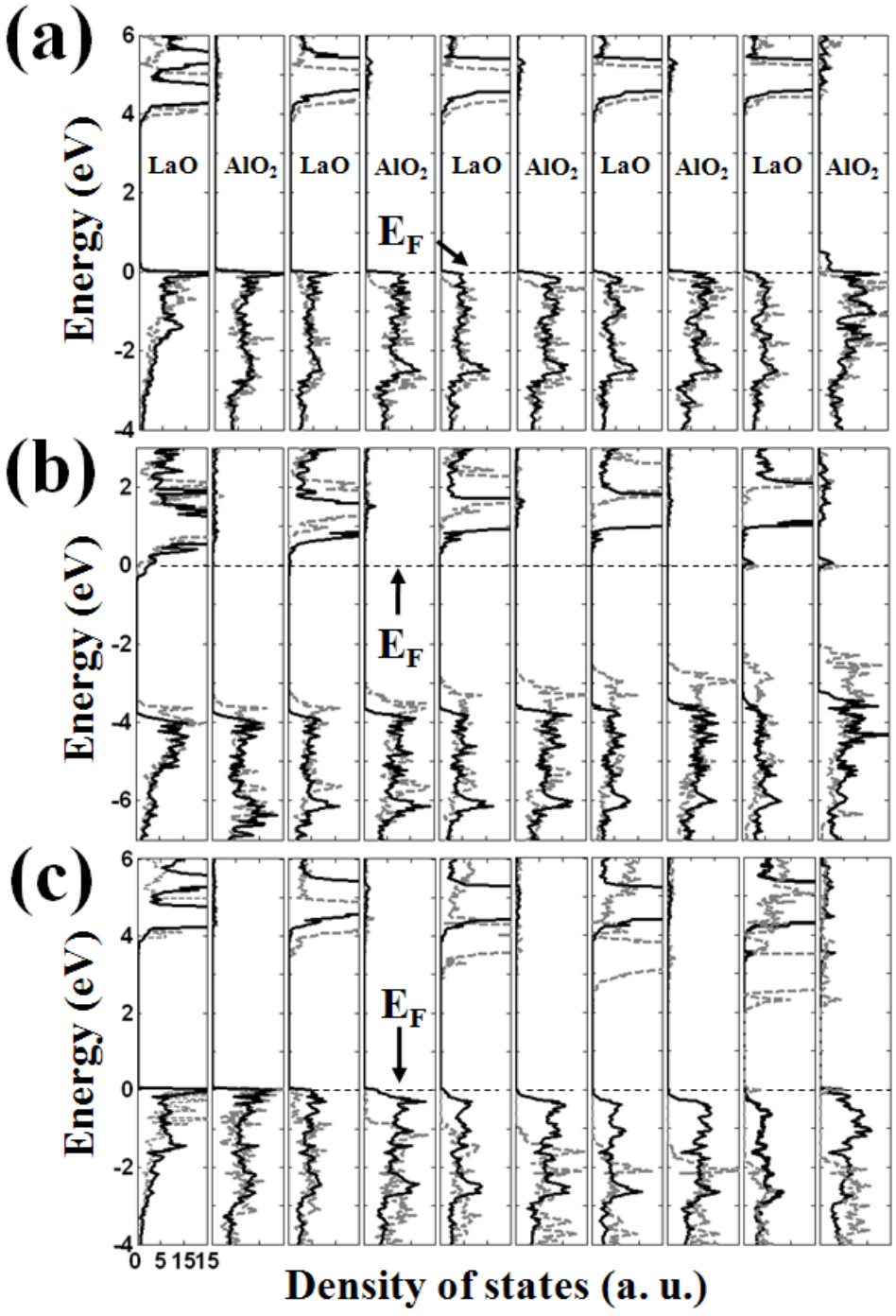

FIG. 9.

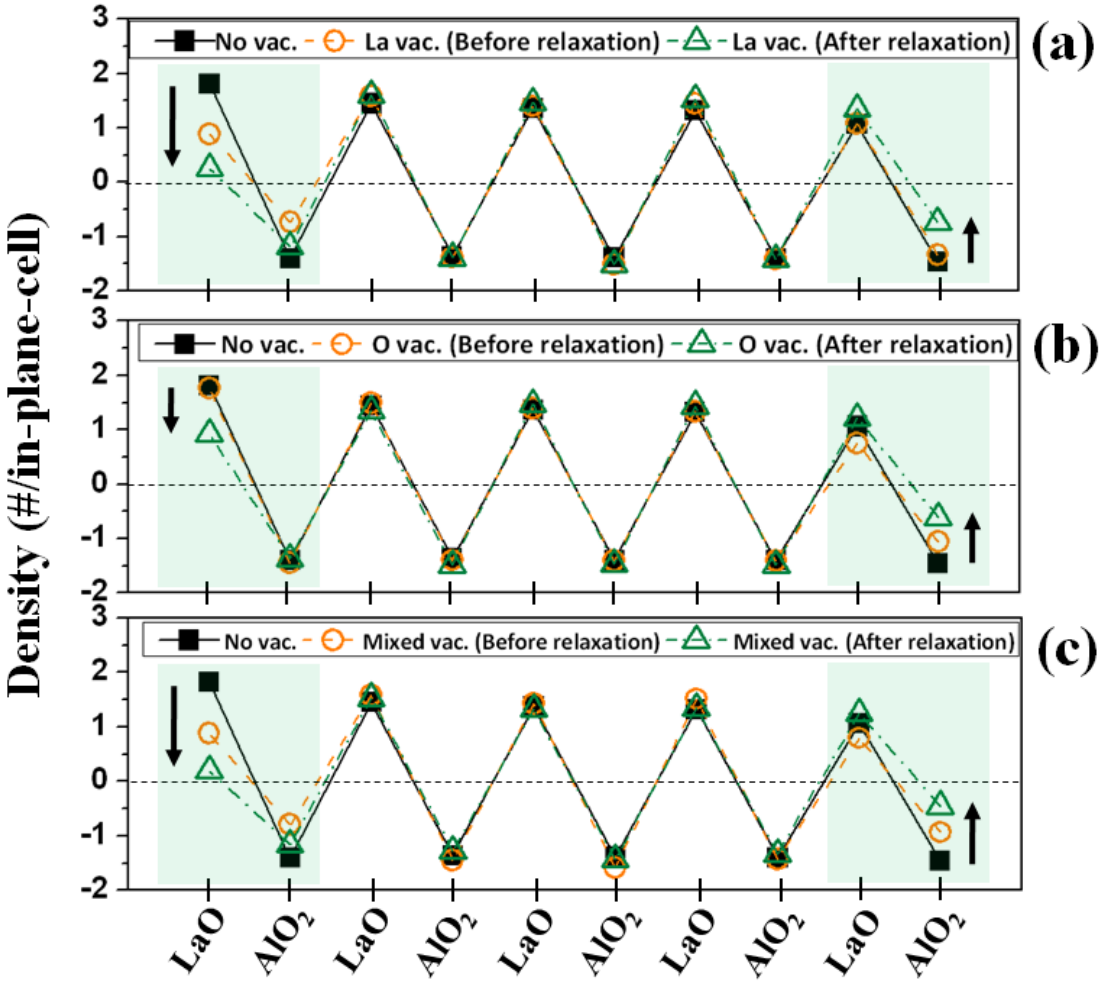
Density (#/in-plane-cell)
No vac.
La vac. (Before relaxation)
La vac. (After relaxation)
(a)
No vac.
O vac. (Before relaxation)
O vac. (After relaxation)
(b)
No vac.
Mixed vac. (Before relaxation)
Mixed vac. (After relaxation)
(c)
LaO
AlO2
LaO
AlO2
LaO
AlO2
LaO
AlO2
LaO
AlO2

FIG. 10.

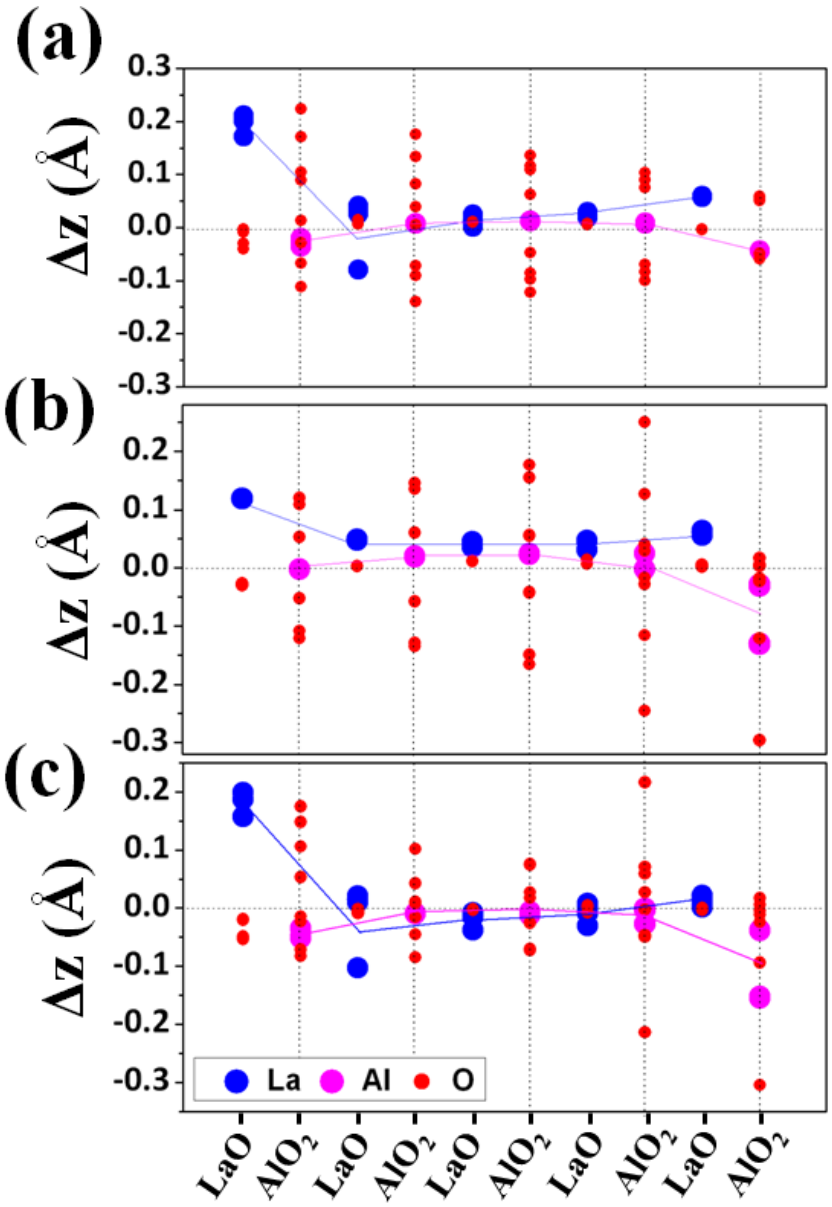

FIG. 11.

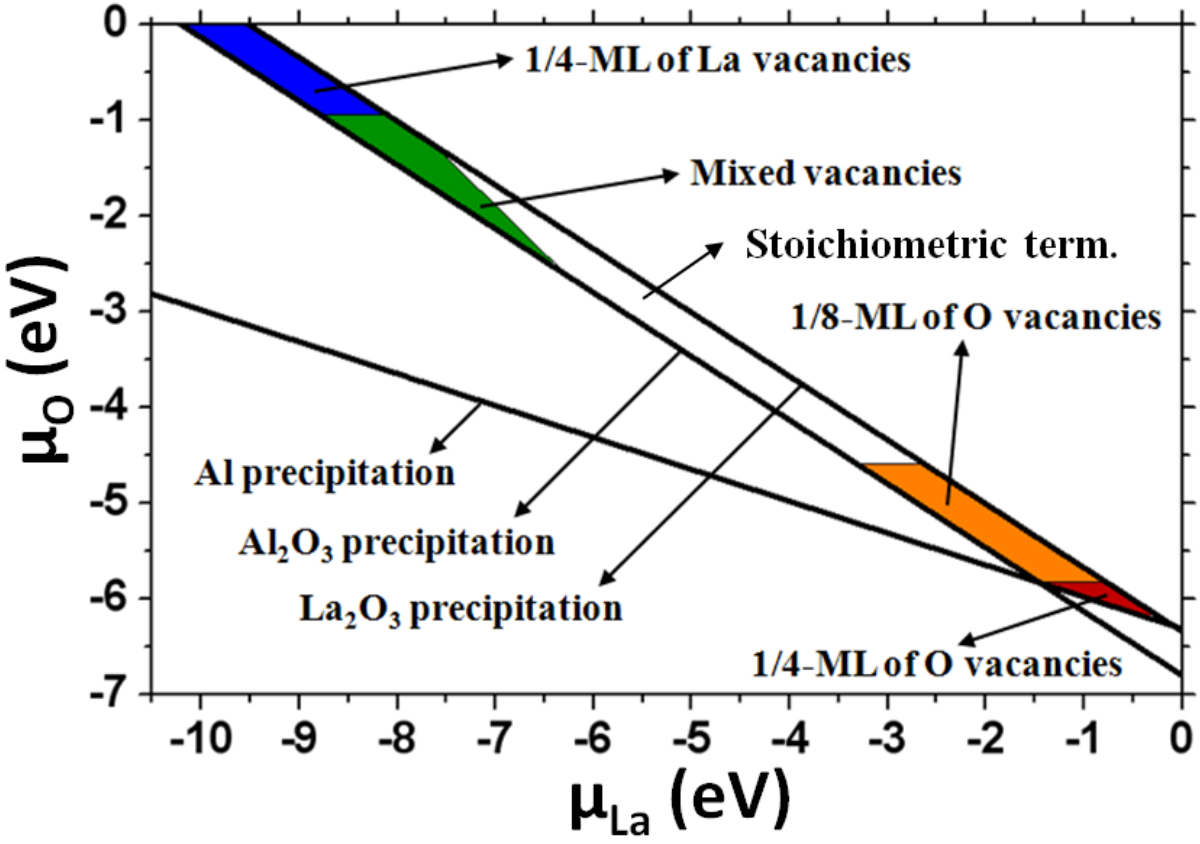
1/4-ML of La vacancies
Mixed vacancies
Stoichiometric term.
1/8-ML of O vacancies
Al precipitation
Al2O3 precipitation
La2O3 precipitation
1/4-ML of O vacancies
μO (eV)
μLa (eV)
0
-1
-2
-3
-4
-5
-6
-7
-10
-9
-8
-7
-6
-5
-4
-3
-2
-1
0

FIG. 12.